

An Analytic Model for the Evolution of the Stellar, Gas, and Metal Content of Galaxies

Romeel Davé¹, Kristian Finlator², Benjamin D. Oppenheimer³

¹ *Astronomy Department, University of Arizona, Tucson, AZ 85721, USA*

² *Hubble Fellow; Physics Department, University of California, Santa Barbara, CA 93106, USA*

³ *Veni Fellow; Leiden Observatory, Leiden University, PO Box 9513, 2300 RA Leiden, Netherlands*

16 November 2011

ABSTRACT

We present an analytic formalism that describes the evolution of the stellar, gas, and metal content of galaxies. It is based on the idea, inspired by hydrodynamic simulations, that galaxies live in a slowly-evolving equilibrium between inflow, outflow, and star formation. We argue that this formalism broadly captures the behavior of galaxy properties evolving in simulations. The resulting equilibrium equations for the star formation rate, gas fraction, and metallicity depend on three key free parameters that represent ejective feedback, preventive feedback, and re-accretion of ejected material. We schematically describe how these parameters are constrained by models and observations. Galaxies perturbed off the equilibrium relations owing to inflow stochasticity tend to be driven back towards equilibrium, such that deviations in star formation rate at a given mass are correlated with gas fraction and anti-correlated with metallicity. After an early gas accumulation epoch, quiescently star-forming galaxies are expected to be in equilibrium over most of cosmic time. The equilibrium model provides a simple intuitive framework for understanding the cosmic evolution of galaxy properties, and centrally features the cycle of baryons between galaxies and surrounding gas as the driver of galaxy growth.

1 INTRODUCTION

Galaxy formation involves a wide range of diverse physical processes operating on stellar to cosmological scales, including the hierarchical growth of structure, star formation, black hole accretion, and a plethora of poorly-understood feedback processes that strongly modulate galaxy growth. Given this complexity, it is surprising that galaxies display simple and tight scaling relations between many of their key constituents. These include well-established relations between the bulge velocity dispersion and central black hole mass (e.g. Gültekin et al. 2009; Graham et al. 2011), circular velocity and luminosity (Tully & Fisher 1977), star formation rate and stellar mass (e.g. Davé 2008; González et al. 2010, and references therein), and metallicity and stellar mass (e.g. Tremonti et al. 2004; Erb et al. 2006). Each has low scatter and evolves roughly independently of mass. The simplicity of these relations hints at an underlying uniformity in galaxy evolution that is not immediately evident from the complexity of current hierarchical galaxy formation models.

In the longstanding canonical scenario for galaxy formation, galaxies form as angular momentum-conserving disks cooling from hot gas bound within dark matter halos, and these disks subsequently merge to form larger and earlier-type galaxies (Rees & Ostriker 1977; White & Rees 1978; White & Frenk 1991; Mo, Mao, & White 1998). This sce-

nario is well-situated within currently favored hierarchical cosmologies, and analytic models based on it have been quite successful at reproducing many observed galaxy properties (see review by Benson 2010). However, the present generation of such models (often called “semi-analytic” models) are typically enormously complex, with a host of free parameters describing various interrelated physical phenomena. Numerical simulations that explicitly track gas dynamical processes enable a more ab initio calculation, but still require many “sub-grid” parameters for key physical processes and are in practice limited by dynamic range and numerical uncertainties. In either case, the complexity of such models makes it difficult to extract simple physical intuition for what drives the evolution of basic galaxy properties.

In this paper, we present an analytic framework for understanding the evolution of the stellar, gas, and metal content of galaxies. This framework is based on intuition gained from hydrodynamic simulations of galaxy formation. In such models, galaxies are fed primarily by cold ($\sim 10^4$ K) streams connecting to filamentary large-scale structure (Kereš et al. 2005; Dekel et al. 2009), outflows are strong and ubiquitous (Springel & Hernquist 2003b; Oppenheimer & Davé 2008), and outflowing material commonly returns to galaxies (“wind recycling”; Oppenheimer et al. 2010). Hence in this framework, galaxy evolution is governed by the cycle of baryons exchanging matter and energy between galaxies and surrounding intergalactic gas.

Our framework is an attempt to distill the insights gained from such hydrodynamic simulations into an analytic formalism that both describes the results of simulations and provides intuition into the key physical drivers. It is based primarily on the formalism presented in Finlator & Davé (2008), with key extensions, and shares features with various recent works (e.g. Rasera & Teyssier 2006; Bouché et al. 2010; Dutton et al. 2010; Krumholz & Dekel 2011), indicating a groundswell towards this “baryon cycling”¹ view of galaxy formation. We demonstrate that the star formation rate, gas content, and metallicity of galaxies can be described by simple equations that depend on three parameters that are directly related to inflows, outflows, and wind recycling. These parameters are poorly constrained in both value and functional form, and hence the number of free parameters in this model may be much greater than three, pending observations that can better constrain them. Together, these parameters quantify the impact of baryon cycling on galaxy growth. We give examples of how these equations lead to straightforward intuitive explanations, often differing from traditional ones, for the results seen in recent observations and models of galaxy evolution.

This paper begins in §2 by describing the basis for our analytic framework, namely the equilibrium condition, and discusses the physical constraints on its various terms that ultimately govern stellar growth. In §3 we present an expression for gas fractions and explore some implications. §4 discusses what governs galaxy metallicities, and relates this to wind recycling. §5 gives some brief examples of how these equilibrium relations yield straightforward intuition into what governs basic galaxy properties. §6 discusses a preliminary implementation of an equilibrium model, and explores some parameter variations. §7 considers what happens when galaxies depart from equilibrium owing both to stochastic fluctuations and more permanent departures. §8 discusses when galaxies first attain equilibrium in the early universe. Finally, we summarize and discuss broader implications of our framework in §9.

2 THE EQUILIBRIUM CONDITION

Star-forming galaxies in hydrodynamic simulations are usually seen to lie near the *equilibrium condition* (see e.g. Figure 13 of Finlator & Davé 2008, and Dutton et al. 2010; Bouché et al. 2010):

$$\dot{M}_{\text{in}} = \dot{M}_{\text{out}} + \dot{M}_{*}, \quad (1)$$

where the terms are the mass inflow rate, mass outflow rate, and star formation rate (SFR), respectively. Inflow and outflow refer to gas motion in and out of the galaxy’s star-forming region, i.e. the interstellar medium (ISM). Star-forming galaxies fluctuate around this relation but are generally driven back to it on short timescales, as we discuss in §7; this “self-regulating” behavior is why we dub this model the *equilibrium model*.

The equilibrium condition is close to an expression for mass conservation, except that it importantly does not contain a term describing a gas reservoir. A key ansatz of this

formalism is that the rate of change in the gas reservoir is small compared to the other terms in Equation 1. The motivation for this ansatz is that in Finlator & Davé (2008), we found this to be explicitly true in hydrodynamic simulations of galaxy formation. We note that this scenario has also been referred to as a “reservoir” or “bath tub” model (Bouché et al. 2010; Krumholz & Dekel 2011).

Defining the mass loading factor $\eta \equiv \dot{M}_{\text{out}}/\dot{M}_{*}$, we can rewrite the equilibrium condition as

$$\text{SFR} = \dot{M}_{\text{in}}/(1 + \eta). \quad (2)$$

Hence in this scenario, a galaxy’s star formation history over cosmic timescales is determined by the evolution of \dot{M}_{in} and η .

Let us consider inflow first. \dot{M}_{in} can be broadly separated into three terms:

- \dot{M}_{grav} = Baryonic inflow into galaxy’s halo, which is primarily set by the assumed cosmology. Here we employ the form forwarded by Dekel et al. (2009):

$$\frac{\dot{M}_{\text{grav}}}{M_{\text{halo}}} = 0.47 f_b \left(\frac{M_{\text{halo}}}{10^{12} M_{\odot}} \right)^{0.15} \left(\frac{1+z}{3} \right)^{2.25} \text{Gyr}^{-1}. \quad (3)$$

Fakhouri, Ma, & Boylan-Kilchin (2010) presented a different parameterization of $25.3 M_{\text{halo}}^{0.1} (1 + 1.65z) \sqrt{\Omega_m (1+z)^3 + \Omega_{\Lambda}} M_{\odot}/\text{yr}$, while Faucher-Giguere, Kereš, & Ma (2011) found $33.6 M_{\text{halo}}^{0.06} (1 + 0.91z) \sqrt{\Omega_m (1+z)^3 + \Omega_{\Lambda}} M_{\odot}/\text{yr}$; these yield similar results over most of cosmic time.

- \dot{M}_{prev} = The amount of the gas entering the halo that is *prevented* from reaching the ISM (to be subtracted from the halo infall). This is material that ends up in the gaseous halo of the galaxy, and can also be regarded as the rate of growth of halo gas. We characterize this by defining a *preventive feedback parameter*

$$\zeta \equiv 1 - \dot{M}_{\text{prev}}/\dot{M}_{\text{grav}}. \quad (4)$$

- \dot{M}_{recyc} = Gas infalling that has previously been ejected in outflows, along with gas returned to the ISM via stellar evolution. This provides an extra component in addition to the baryons associated with the gravitational infall of dark matter (i.e. \dot{M}_{grav}).

Expressing \dot{M}_{in} in these terms, we obtain

$$\dot{M}_{\text{in}} = \dot{M}_{\text{grav}} - \dot{M}_{\text{prev}} + \dot{M}_{\text{recyc}} = \zeta \dot{M}_{\text{grav}} + \dot{M}_{\text{recyc}} \quad (5)$$

Halo infall (\dot{M}_{grav}) is driven by gravity, hence is mostly independent of feedback processes (van de Voort et al. 2011; Faucher-Giguere, Kereš, & Ma 2011) and is determined primarily by cosmology and the halo merger rate (e.g. Neistein, van den Bosch, & Dekel 2006; Neistein & Dekel 2008; McBride, Fakhouri, & Ma 2009; Genel et al. 2010). In contrast, \dot{M}_{prev} and \dot{M}_{recyc} are direct consequences of feedback processes. We will discuss \dot{M}_{recyc} further in §4, when we will relate it to the metallicity of the infalling gas. This leaves the preventive feedback parameter ζ , which we now consider.

There are a number of sources of preventive feedback, each with its own dependence on halo mass and redshift, the products of which comprise the total ζ :

- ζ_{photo} represents suppression of inflow owing to photo-ionisation heating. This operates at low masses, and approaches zero below a *photo-suppression mass* that increases

¹ A term coined in the Astro2010 Decadal Survey Report: New Worlds, New Horizons

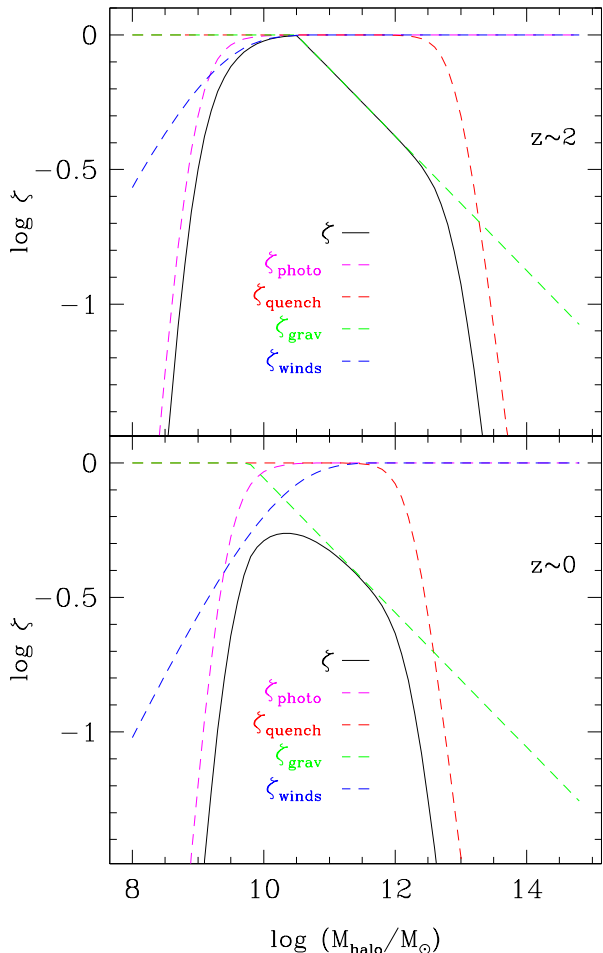


Figure 1. Schematic illustration of the preventive feedback parameter $\zeta(M_{\text{halo}})$. ζ_{photo} (magenta) is parameterized here as $(1 + \frac{1}{3}(M/M_\gamma)^{-2})^{-1.5}$ (following eq. 1 of Okamoto, Gao, & Theuns 2008), and ζ_{quench} (red) is analogously parameterized. ζ_{grav} (green) is taken from Equation 6. ζ_{winds} (blue) is an arbitrary function depicting an increasing effect to smaller masses from wind heating. *Top panel:* We choose $M_\gamma = 10^9 M_\odot$ and $M_q = 10^{13} M_\odot$, perhaps appropriate for $z = 2$. *Bottom panel:* We choose $M_\gamma = 3 \times 10^9 M_\odot$, $M_q = 10^{12.3} M_\odot$, and a stronger ζ_{winds} , more appropriate for $z = 0$. These values and their parameterizations are fairly arbitrary, because the terms are poorly constrained; this plot is purely intended to illustrate general trends. The total $\zeta = \zeta_{\text{photo}}\zeta_{\text{quench}}\zeta_{\text{grav}}\zeta_{\text{winds}}$ is shown as the black line, showing that vigorous star formation can only proceed within an intermediate range of halo masses where ζ approaches unity.

from a halo mass of $M_\gamma \sim 10^8 M_\odot$ during reionisation to $M_\gamma \sim \text{few} \times 10^9 M_\odot$ at the present epoch (Gnedin 2000; Okamoto, Gao, & Theuns 2008).

- ζ_{quench} is associated with whatever physical process(es) quench star formation in massive halos and prevents cooling flows, probably related to feedback from supermassive black holes (e.g. Somerville et al. 2008). It drops to zero above the *quenching mass* $M_q \sim 10^{12} M_\odot$ (e.g. Croton et al. 2006; Gabor et al. 2011), which may be higher at high- z (Dekel et al. 2009). This may further depend on the merger history of galaxies (Hopkins et al. 2008).

- ζ_{grav} reflects suppression of inflow by ambient gas heating owing to gravitational structure formation via the for-

mation of virial shocks. Using hydrodynamic simulations with no outflows, Faucher-Giguere, Kereš, & Ma (2011) determined

$$\zeta_{\text{grav}} \approx 0.47 \left(\frac{1+z}{4} \right)^{0.38} \left(\frac{M_{\text{halo}}}{10^{12} M_\odot} \right)^{-0.25}. \quad (6)$$

We note that those simulations did not include metal-line cooling, which may be an important effect for heating gas in virial shocks (Dekel & Birnboim 2006; Ocvirk, Pichon, & Teyssier 2008); nonetheless, we show in Figure 2 that our simulations including metal-line cooling yield similar results.

- ζ_{winds} is associated with additional heating of surrounding gas provided by energetic input from winds. This tends to affect lower-mass systems more, but is highly dependent on the physics of how outflows interact with surrounding gas, which is poorly understood. Recent results (Oppenheimer et al. 2010; van de Voort et al. 2011; Faucher-Giguere, Kereš, & Ma 2011) have demonstrated that this can be a significant effect in plausible (though somewhat extreme) wind models. Note that although both ζ_{winds} and η arise from winds, the former is a preventive feedback parameter, whereas η is an ejective feedback parameter; the two are not necessarily related in a simple way, so we keep them separate.

Multiplying these terms together, we obtain $\zeta(M_{\text{halo}})$ that is schematically illustrated in Figure 1. It is small at low and high halo masses owing to photo-suppression and quenching respectively, and approaches unity at intermediate halo masses which is where vigorous star formation can occur. This depiction is intended only to illustrate broad trends, as the actual values and functional forms of the various ζ terms are at best only qualitatively known. The general shape of this curve with a cutoff in accretion at low and high masses is long known (e.g. Thoul & Weinberg 1996; Kereš et al. 2005; Croton et al. 2006), although the quantitative masses for the cutoffs are debated to this day (for recent work on this see Bouché et al. 2010; Cattaneo et al. 2011).

There may be other sources of energetic preventive feedback that retard accretion such as cosmic rays, stellar winds, quasar outflows, local photo-ionisation, and magnetic fields, but their importance for global galaxy evolution has not yet been firmly established. There may also be subtle “amplification” effects by which two or more preventive mechanisms serve to strengthen each other beyond their individual impact (Pawlik & Schaye 2009; Finlator, Davé, & Özel 2011). Hence the list of individual ζ ’s above is intended to illustrate the sort of physical processes contributing to preventive feedback, and how they might manifest in the overall shape of ζ . The actual trend of $\zeta(M_{\text{halo}})$ may involve more complicated and subtle effects than described here.

Figure 2 illustrates the impact of these various inflow and feedback terms on the specific star formation rate ($\text{sSFR} \equiv \text{SFR}/M_*$) as a function of M_{halo} , using large-scale cosmological hydrodynamic simulations with various outflow models (see Davé, Oppenheimer, & Finlator 2011, for details). The upper left panel shows the case without outflows. If all gas entering into the halo ended up in the ISM, i.e. $\dot{M}_{\text{in}} = \dot{M}_{\text{grav}}$, then the relation would be as shown by the solid line, having a positive slope. Even without any feedback, gravitational heating results

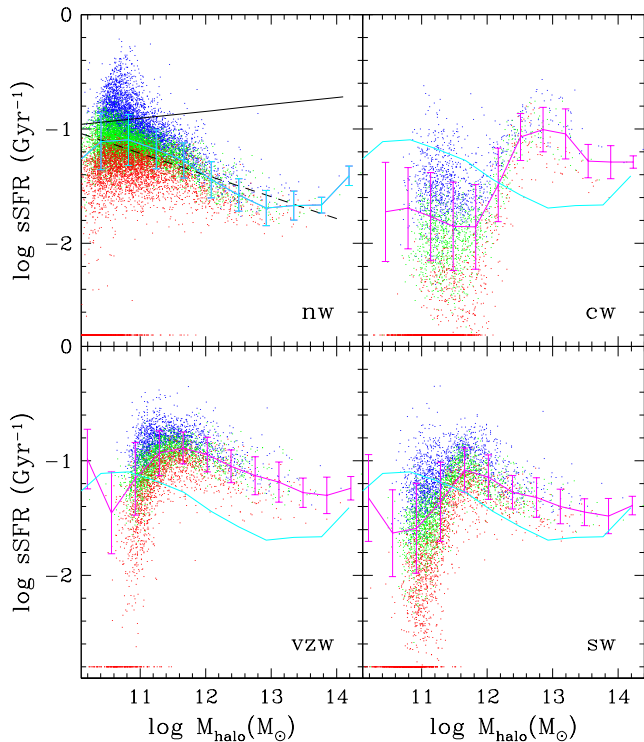


Figure 2. Specific star formation rate (sSFR \equiv SFR/ M_*) versus halo mass M_{halo} at $z = 0$ in 48 Mpc/h cosmological hydrodynamic simulations (see Davé, Oppenheimer, & Finlator 2011, for details). Each point represents a galaxy, and at a given mass these are subdivided into high f_{gas} (blue; $> 0.5\sigma$ above the median), low f_{gas} (red; $< -0.5\sigma$ below the median), and intermediate (green). Upper left panel shows the case with no outflows (nw). Solid black line shows the halo mass scaling of \dot{M}_{grav} from Fakhouri, Ma, & Boylan-Kilchin (2010), while dashed line shows the effect of gravitational preventive feedback (eq. 6, and Faucher-Giguere, Kereš, & Ma 2011). The cyan line shows a running median; this curve is reproduced in the other panels for comparison. The upper and lower right panels show models where we assume $\eta = 2$ and $v_{\text{wind}} = 680$ km/s and 340 km/s (cw and sw), respectively. The lower left panel shows momentum-driven wind scalings (vzw; Murray, Quataert, & Thompson 2005), in which $\eta \propto M_{\text{halo}}^{-1/3}$ and the outflow speed is $\propto M_{\text{halo}}^{1/3}$ (roughly). Deviations from the no-wind case represent the influence of other terms on \dot{M}_{in} , particularly \dot{M}_{recyc} at high masses and ζ_{winds} at low masses.

in a negative slope (dashed line). The results from our simulations are in good agreement with Equation 6 (from Faucher-Giguere, Kereš, & Ma 2011), since the simulations themselves are quite similar; the main difference is that ours include metal-line cooling, but this is not very important until hot gaseous halos form at $M_{\text{halo}} \gtrsim 10^{12} M_{\odot}$ (Kereš et al. 2005; Gabor et al. 2011) since cold accretion is generally limited by the infall time rather than the cooling time.

The simulations in the two right panels assume $\eta = 2$. If \dot{M}_{in} is unchanged, then one expects both the SFR and M_* to be lowered by a factor of three (eq. 2), resulting in no change in sSFR from the no-wind case (the no-wind cyan curve is reproduced in all panels for comparison). But clearly there is a change, which reflects the impact of outflows on \dot{M}_{in} . At large masses, wind recycling (\dot{M}_{recyc}) returns material to the galaxy rapidly once the wind speed (680 km/s in the upper

right, 340 km/s in the lower right) drops below the escape velocity (Oppenheimer et al. 2010). Hence at large masses η is effectively 0 (Finlator & Davé 2008), and sSFR jumps owing to \dot{M}_{recyc} . For the case of the slower 340 km/s winds (lower right), the jump occurs at a factor of eight lower in mass as expected from the factor of two difference in wind speeds. Winds also affect sSFR at low masses, where it is suppressed relative to no winds. This reflects ζ_{winds} , which is as expected stronger in the case of the higher wind speed. In the lower left we show simulations using momentum-driven wind scalings of (approximately) $\eta \propto M_{\text{halo}}^{-1/3}$. This flattens sSFR(M_{halo}), in addition to exhibiting different behaviors for wind recycling and suppression.

These examples illustrate how star formation rates at a given mass in simulations are impacted by the various ejective and preventive feedback processes described above. For instance, the fact that observations find no sudden increase in sSFR at any characteristic mass (e.g. Salim et al. 2007; Daddi et al. 2007) suggests that galaxies do not eject material at a characteristic wind velocity.

Bouché et al. (2010), Dutton et al. (2010), and Krumholz & Dekel (2011) also present empirical models based on accretion-driven star formation, focusing on the form and evolution of the sSFR. Interestingly, Bouché et al. (2010) demonstrates that a model in which $\zeta = 1$ for $10^{11} < M_{\text{halo}} < 10^{12.2} M_{\odot}$ and zero elsewhere nicely reproduces some key observed properties of high-redshift star-forming galaxies, including the observed lack of sSFR amplitude evolution from $z \sim 7 \rightarrow 2$. Simulations, in contrast, predict that sSFR evolution tracks the accretion rate, and thus continues to rise to high redshifts (Davé 2008); analytic models that do not include such a low-mass cutoff show similar behavior (Dutton et al. 2010). If this low-mass cutoff for accretion were true, it would suggest that there are additional feedback processes affecting small systems beyond what is shown in Figure 1, namely, metagalactic photo-ionisation. An alternative explanation that does not employ a sharp mass cutoff but still reproduces the observed sSFR behavior is to invoke an observationally-motivated metallicity-dependent star formation law, as explored by Krumholz & Dekel (2011). Pushing such observations of sSFR out to higher redshifts and lower masses (e.g. with the Cosmic Assembly Near-Infrared Deep Legacy Survey; Grogin et al. 2011; Koekemoer et al. 2011) should provide interesting constraints on the physical mechanisms regulating early, low-mass galaxy growth.

3 GAS FRACTIONS

A galaxy’s gas fraction is defined here as

$$f_{\text{gas}} \equiv \frac{M_{\text{gas}}}{M_{\text{gas}} + M_*} = \frac{1}{1 + (t_{\text{dep}} \text{sSFR})^{-1}} \quad (7)$$

where in the second equality we have employed the *depletion time* $t_{\text{dep}} \equiv M_{\text{gas}}/\text{SFR}$. We argue below that the latter formulation offers the intuitive advantage that it splits f_{gas} into a term that is fairly insensitive to feedback (t_{dep}) and a term that depends strongly on feedback (sSFR).

The depletion time measures the timescale over which gas, when present in the ISM, gets converted into stars. This is expected to be primarily determined by the star formation

law, such as the observed Kennicutt (1998) relation between gas surface density (Σ_{gas}) to SFR surface density (Σ_{SFR}). Indeed, simulations by Davé, Finlator, & Oppenheimer (2011, hereafter DFO11; see their Figure 4) assuming a Kennicutt-Schmidt law show that t_{dep} is essentially independent of outflows, and scales as

$$t_{\text{dep}} \propto t_H M_*^{-0.3}, \quad (8)$$

where t_H is the Hubble time.

We can derive this scaling of t_{dep} directly from the star formation law. The temporal scaling can be most easily understood using a formulation of the star formation law given by $\text{SFR} \approx 0.02 M_{\text{gas}}/t_{\text{dyn}}$, where t_{dyn} is the dynamical time of the star formation region (e.g. Silk 1997; Krumholz & Tan 2007; Genzel et al. 2010). This then gives $t_{\text{dep}} \propto t_{\text{dyn}}$, which in a canonical disk model scales as the Hubble time t_H (Mo, Mao, & White 1998). Meanwhile, the stellar mass dependence arises from the Kennicutt law plus the ISM gas profile. The Kennicutt law states that $\Sigma_{\text{SFR}} \propto \Sigma_{\text{gas}}^N$ (where $N \approx 1.4$), from which it is straightforward to show that $t_{\text{dep}} \propto \Sigma_{\text{gas}}^{1-N}$. In simulations, $\Sigma_{\text{gas}} \propto M_*^{3/4} (1+z)^2$ (DFO11), which gives rise to the weak anti-correlation with M_* quoted above. We caution that these dependences may be somewhat different in the real Universe since these simulations lack the resolution to properly model the internal structure of galaxies.

The evolution of f_{gas} depends on the evolution of t_{dep} and sSFR. The former evolves with t_H (e.g. as $(1+z)^{-1.5}$ in the matter-dominated regime), while the latter is generally driven by cosmic inflow (eq. 3) which scales as $(1+z)^{2.25}$ if driven by gravitational infall. Combining these, galaxy gas fractions are predicted to evolve with time roughly as $\sim (1+z)^{2.25} t_H$ (if f_{gas} is not near unity), which increases slowly with redshift, qualitatively consistent with observations (Tacconi et al. 2010; Geach et al. 2011). Hence in the equilibrium scenario, galaxy gas fractions represent a competition between supply and consumption, such that *galaxies become less gas-rich with time because the gas supply rate drops faster than the gas consumption rate.*

4 METALLICITIES

The global metallicity within the ISM is given by the enrichment rate, which is the yield y times SFR, divided by the mass inflow rate \dot{M}_{in} that must be enriched. As derived in Finlator & Davé (2008), if the inflow is pre-enriched there is an additional term that depends on $\alpha_Z \equiv Z_{\text{in}}/Z_{\text{ISM}}$, where Z_{in} and Z_{ISM} are the metallicities of the inflowing and ambient ISM gas, respectively:

$$Z_{\text{ISM}} = y \frac{\text{SFR}}{\dot{M}_{\text{in}}} = \frac{y}{1+\eta} \frac{1}{1-\alpha_Z}. \quad (9)$$

Hence the mass-metallicity relation and its evolution are established by a the mass and redshift dependence of η and α_Z . In our currently favored outflow model (Davé, Oppenheimer, & Finlator 2011), η has a significant mass dependence but little or no redshift dependence, while α_Z is generally small but has a significant redshift dependence. Equation 9 would then suggest that the shape of the mass-metallicity relation is primarily established by $\eta(M_*)$, while its evolution is driven by α_Z ; this was

demonstrated for simulations in DFO11. Hence in this scenario, *the shape of the mass-metallicity relation is modulated by the fraction of inflow that forms stars, while its evolution is governed by the enrichment level of infalling gas.*

Conspicuously absent in this scenario is any explicit reference to potential wells of galaxies, or any consideration of outflow velocities versus escape velocities. These processes are canonically believed to govern the mass-metallicity relation (e.g. Dekel & Silk 1986; Tremonti et al. 2004); the phrase “metals can more easily escape from the shallower potential wells of small galaxies” is oft-repeated. However, in our scenario, it is instead the net mass outflow rate that is the key determinant of the mass-metallicity relation, and the potential well depth is at most only indirectly implicated.

Since the vast majority of metals in the IGM are deposited there by outflows (e.g. Oppenheimer & Davé 2008; Oppenheimer et al. 2011), the infalling gas metallicity is a direct measure of \dot{M}_{recyc} . Z_{in} is given by the metal mass arriving in the form of recycled winds, divided by the total mass inflow rate, i.e.

$$Z_{\text{in}} = Z_{\text{recyc}} \frac{\dot{M}_{\text{recyc}}}{\dot{M}_{\text{recyc}} + \zeta \dot{M}_{\text{grav}}}, \quad (10)$$

where the denominator is \dot{M}_{in} from Equation 5.

Under the typical case of highly mass-loaded outflows, the outflowing metallicity must be similar to the ambient ISM metallicity, i.e. $Z_{\text{out}} \approx Z_{\text{ISM}}$. Furthermore, since galaxies evolve slowly in metallicity (e.g. Brooks et al. 2007, DFO11) and wind recycling times are typically of order a Gyr (Oppenheimer et al. 2010), the galaxy metallicity has probably not evolved strongly from when the gas was ejected to when it is being re-accreted, and hence $Z_{\text{recyc}} \approx Z_{\text{out}}$. Substituting $Z_{\text{recyc}} = Z_{\text{ISM}}$ into Equation 10 and solving for \dot{M}_{recyc} yields

$$\dot{M}_{\text{recyc}} = \frac{\alpha_Z}{1-\alpha_Z} \zeta \dot{M}_{\text{grav}}. \quad (11)$$

This relates the mass recycling term in the inflow equation (eq. 2) to the metallicity infalling into the ISM. The advantage of formulating recycling in terms of α_Z is that it is in principle an observable quantity via absorption or emission measures in the outskirts of galaxies. In contrast, \dot{M}_{recyc} is not directly measurable since it is not clear how to distinguish recycled wind inflow from other inflow, or even how to measure galaxy inflow rates at all. Note that since galaxy metallicities evolve slowly upwards with time, Equation 11 will tend to slightly underestimate \dot{M}_{recyc} for a given α_Z . The ejection of winds from one galaxy (typically a satellite) being accreted onto another (typically the associated central) could also affect α_Z , which would also cause an underestimate in \dot{M}_{recyc} since the satellites are generally smaller and hence lower metallicity.

5 THE EQUILIBRIUM RELATIONS & IMPLICATIONS

We can substitute Equation 11 into Equation 5 to obtain

$$\text{SFR} = \frac{\zeta \dot{M}_{\text{grav}}}{(1+\eta)(1-\alpha_Z)}. \quad (12)$$

This is the key equation that delineates how galaxy star formation rates are governed by accretion and feedback

processes, i.e. baryon cycling. This equation, together with Equations 7 and 9, represent the *equilibrium relations* that govern the stellar, gas, and metal content of galaxies across cosmic time. Galaxies will tend to lie around these relations owing to a balance of inflow, outflow, and star formation.

The equilibrium relations depend on three parameters: η , ζ , and α_Z , representing ejective feedback (i.e. outflows), preventive feedback, and wind recycling. Additionally, the star formation law governs t_{dep} , \dot{M}_{grav} is set by cosmology, and y is set by nucleosynthetic processes. Assuming those are well-established, the mass and redshift (and possibly environmental) dependence of η , ζ , and α_Z govern the evolution of the global SFR, f_{gas} , and Z_{ISM} of galaxies. Note that since the mass and redshift dependence of these parameters are not fully known, the actual number of free parameters can be significantly larger than three.

There are many possible ways to characterize simulation results into an analytic formalism (e.g. Neistein et al. 2011). One virtue of our particular parameterization is that the parameters involved are, at least in principle, directly observable. This provides an optimally direct connection from observations to constraints on galaxy formation models. Unfortunately, measuring these parameters is challenging, but preliminary constraints have already been obtained.

For instance, η has been constrained in high- z galaxies to have a value of order unity or more (e.g. Steidel et al. 2010; Genzel et al. 2011). α_Z can be constrained by examining metallicities in the outskirts of low- z galaxies (e.g. Bresolin et al. 2009; Moran et al. 2011). Constraining ζ by direct observations would require an accurate census of all halo gas which is highly challenging, but aside from ζ_{winds} , its main terms can be constrained using a combination of relatively straightforward numerical work (ζ_{photo} and ζ_{grav}) and empirical arguments (ζ_{quench}).

The equilibrium relations have some interesting implications for the behavior of SFR, f_{gas} , and Z . For instance, hydrodynamic simulations indicate that the star formation history of galaxies is insensitive to the assumed star formation law (Katz et al. 1996; Schaye et al. 2010). This seems paradoxical at first, but is straightforwardly seen from Equation 12, since there is no dependence here (or in the metallicity equation) on the star formation law. The star formation law only affects the gas fractions, via t_{dep} . This can be regarded as a self-regulation mechanism (Schaye et al. 2010), in which gas collects in galaxies as required in order to achieve the star formation rate set by the balance of inflows and outflows.

Another straightforward prediction of the equilibrium relations is that if one desires the mass-metallicity relation to scale as $Z \propto M_*^{1/3}$ at small masses as observed (Tremonti et al. 2004; Lee et al. 2006), then Equation 9 directly implies $\eta \propto M_*^{-1/3}$ (assuming $\alpha_Z \ll 1$), roughly as expected for momentum-driven winds (Murray, Quataert, & Thompson 2005). Indeed, simulations assuming such a scaling appear to provide a good match to mass-metallicity relation observations (Finlator & Davé 2008, DFO11).

It is instructive to combine Equations 9 and 12 to give

$$\zeta = \frac{\text{SFR}}{\dot{M}_{\text{grav}}} \frac{y}{Z_{\text{ISM}}} \quad (13)$$

The first ratio is the *halo star formation efficiency* (SFE),

i.e., the fraction of gravitational infall into a halo that ends up forming into stars², while the second ratio quantifies the metal retention fraction within galaxies. If the halo mass and metal yield can be determined, measuring SFR/ Z_{ISM} provides a quantitative constraint on ζ . This can be done at least at $z \sim 0$ with existing data from e.g. the Sloan Digital Sky Survey.

6 A SAMPLE EQUILIBRIUM MODEL

The equilibrium model can be used to quickly explore parameter space and obtain intuition about the governing physics for galaxy properties of interest. We illustrate this here by presenting results for the evolution of galaxies in a full equilibrium model.

Figure 3 shows the evolution of the SFR, halo SFE, Z , and f_{gas} for four galaxies spanning the indicated range of final ($z = 0$) halo masses. These are computed using Equations 7, 9, and 12, tracking the stellar and halo mass growth starting at an early epoch when the halo is at the photo-suppression mass. We take \dot{M}_{grav} from Equation 3, parameterize $t_{\text{dep}} = 0.4t_H(M_*/10^{10}M_\odot)^{-0.3}$ as discussed in §3, and take $\alpha_Z = (0.5 - 0.1z)(M_*/10^{10}M_\odot)^{0.25}$ (with $\alpha_Z \geq 0$) as a crude parameterization of simulation results from DFO11. We choose ζ as described in Figure 1, and define η as indicated in the upper right of the Figure: solid lines approximately represent momentum-driven wind scalings, while dotted lines represent energy-conserving wind scalings. We also include instantaneous recycling of 18% of star formation back into gas as expected for a Chabrier (2003) IMF, but do not include further stellar mass loss. We reiterate that these “base model” parameter choices are at some level arbitrary, and are intended only to illustrate how parameter variations influence observables.

The green line represents a Milky Way-sized halo of $10^{12}M_\odot$. At $z = 0$, it has SFR $\approx 2.5M_\odot/\text{yr}$, $M_* \approx 5 \times 10^{10}M_\odot$, $f_{\text{gas}} \approx 0.1$, and $Z \approx Z_\odot$, in fair agreement with measured values and showing that our parameter choices are reasonable. Larger galaxies form stars more vigorously at earlier epochs and for shorter intervals, which is qualitatively similar to the behavior in the empirical “staged” galaxy formation model of Noeske et al. (2007). The peak SFRs are 50–100 M_\odot/yr at $z \sim 2 - 3$, which is lower than the observed values for the largest main sequence galaxies at that epoch by a factor of a few, reiterating the issue noted in simulations by Davé (2008) that observed galaxy SFRs at that epoch approach or exceed their cosmic accretion rate; the resolution to this quandary remains unclear (see e.g. Bouché et al. 2010; Krumholz & Dekel 2011, for ideas).

The halo SFE is plotted in the second panel. For star-forming galaxies, this efficiency is roughly one-third to one-half over most of cosmic time. Higher mass halos show a marked drop in efficiency once they grow above the quenching mass, here assumed to be $2 \times 10^{12}M_\odot$ at all epochs. Going to a steeper scaling of $\eta(M_h) \propto M_h^{-2/3}$ (dotted

² This is distinguished from the ISM SFE, which is how much gas is converted into stars over some characteristic galaxy timescale, or the “cosmological” SFE, which is the galaxy stellar mass divided by the cosmologically-expected halo baryon mass (i.e. $M_*/f_b M_{\text{halo}}$).

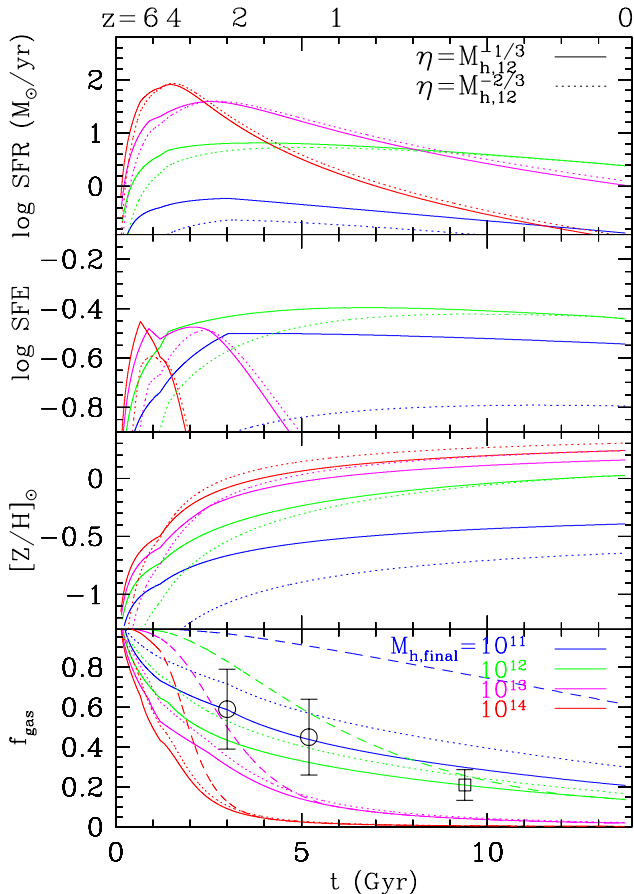


Figure 3. Equilibrium model evolution of four galaxies that have final $z = 0$ halo masses of $10^{11} M_{\odot}$, $10^{12} M_{\odot}$, $10^{13} M_{\odot}$, and $10^{14} M_{\odot}$ (blue, green, magenta, and red lines, respectively). Panels from top to bottom show the star formation rate, cosmic star formation efficiency defined as the fraction of baryons entering the halo that form into stars, gas fractions, and metallicities. Solid lines show $\eta = (M_h/10^{12} M_{\odot})^{-1/3}$, and dotted lines show $\eta = (M_h/10^{12} M_{\odot})^{-2/3}$. The star formation histories peak earlier and at higher SFRs for larger galaxies, reminiscent of the empirical “staged galaxy formation” model of Noeske et al. (2007). Star formation efficiencies are typically $\sim 1/2 - 1/3$ for star-forming galaxies, and drop quickly about the quenching halo mass of $10^{12.3} M_{\odot}$ for more massive systems. Galaxies self-enrich to above one-tenth solar very early on, and then evolve slowly in metallicity. Observed gas fractions for fairly massive galaxies from Tacconi et al. (2010) at $z = 1.2$ and 2.2 and Geach et al. (2011) at $z = 0.4$ are indicated, to be compared with predictions for $\sim 10^{12-13} M_{\odot}$ halos; the model predictions are generally too low. The dashed lines show the experiment of adding a metallicity dependence of $\propto Z^{-2}$ to t_{dep} when sub-solar, which keeps early galaxies gas-rich and improves agreement with data.

lines) more strongly suppresses low-mass galaxy growth, which is favored in semi-analytic models to reproduce the observed faint-end slope of the stellar mass function (e.g. Somerville et al. 2008).

Metallicity evolution is very rapid in all galaxies early on, and galaxies typically enrich to $\gtrsim 0.1 Z_{\odot}$ within the first Gyr, as seen in simulations (Davé et al. 2006; Finlator, Oppenheimer, & Davé 2011). Evolution is slow thereafter. Galaxies tend to follow parallel tracks, showing that the shape of the mass-metallicity relation does not

evolve much (DFO11). A steeper scaling of $\eta(M_h)$ strongly steepens the mass-metallicity relation in smaller galaxies at all redshifts, as expected from Equation 9.

f_{gas} drops slowly with time since the accretion rate drops faster than the consumption rate, as discussed in §3. Here we include some observational comparisons (large symbols), from CO measurements by Tacconi et al. (2010) and Geach et al. (2011). As Tacconi et al. (2010) noted, the relatively slow evolution requires continual replenishment, as our model naturally predicts. However, the $z \sim 1-2$ gas fractions are higher than the model predictions, because the observed galaxies are best compared to the green and magenta lines representing final halo masses of $\sim 10^{12} - 10^{13} M_{\odot}$. The equilibrium model can quickly test whether parameter variations can reconcile this discrepancy.

According to Equation 7, higher f_{gas} values can be achieved by raising sSFR and/or t_{dep} . Raising sSFR e.g. by lowering η would concurrently alleviate the discrepancy with observed $z \sim 2$ SFRs, but would likely overproduce stars globally. Delaying star formation by accumulating gas could explain the discrepancy, though it seems somewhat contrived to have galaxies at all masses suddenly start vigorously consuming gas around $z \sim 2$. A steeper scaling of $\eta(M_h)$ works in this direction, but the dotted lines show that this only helps marginally; a redshift-dependent η that is higher at high- z may work better, but the physical motivation is not obvious. Another avenue is to raise t_{dep} by appealing to the observed lower gas consumption rate in low-metallicity systems (Bolatto et al. 2011). An illustration of this is shown as the dashed lines in Figure 3, where we add a dependence of Z^{-2} to t_{dep} when below solar metallicity. Within this model, we find that this steep metallicity dependence is required in order to sufficiently raise gas fractions at high- z ; however, it is not physically-motivated, and does not necessarily reflect recently proposed metallicity-dependent star formation laws (e.g. Krumholz & Dekel 2011). The delay in star formation results in higher gas fractions at $z \sim 2$ in better agreement with data, but at lower redshifts when metallicities approach solar this makes less difference. Another avenue explored by Bouché et al. (2010) is to postulate that star formation can only occur in halos above $10^{11} M_{\odot}$, which has the advantage of producing higher gas fractions in smaller systems at earlier epochs; they demonstrate that this can broadly match the observed evolution of galaxy gas fractions.

This exercise illustrates how an equilibrium model can be utilized to gain intuition about various physical processes in galaxy evolution. The relatively small number of parameters and their direct connection to observable physical processes makes this type of model easier to interpret than modern simulations or semi-analytic models.

7 DEPARTURES FROM EQUILIBRIUM

Stochastic variations in \dot{M}_{in} , including mergers, can cause departures from equilibrium. This generates scatter about the equilibrium relations. Generically, departures from equilibrium tend to return galaxies towards equilibrium. This self-regulating behavior is why we dub this scenario the equilibrium model.

To illustrate this behavior, consider a galaxy experi-

encing an upward fluctuation in \dot{M}_{in} . Its f_{gas} increases, and perhaps M_* as well if there is a small galaxy accompanying the infall, while Z_{ISM} decreases since either fresh infall or a lower-mass galaxy will have lower metallicity. This moves the galaxy off the equilibrium relations. The increased gas content immediately stimulates more vigorous star formation, which over time enriches the galaxy as it consumes the excess gas. This then lowers its gas content and increases its metallicity, moving the galaxy back towards equilibrium.

Conversely, a temporary lull in accretion will make a galaxy more gas-poor and metal-poor as it consumes its existing gas. Quantitatively, its metallicity will evolve following the relation $\Delta Z_{\text{ISM}} \approx y \Delta M_*/M_{\text{gas}}$ (see eq. 19 of Finlator & Davé 2008, in the case of zero accretion), which is steeper than the MZR and hence will move the galaxy above the MZR. In time, hierarchical growth will bring in fresh gas, lowering the metallicity and increasing the gas content to return the galaxy towards equilibrium. In this way, galaxies oscillate around the equilibrium relations, constantly being perturbed from them and driven back owing to fluctuations in infall.

An inevitable prediction of this scenario is that departures from the equilibrium relations will correlate with star formation rate, gas fraction, and metallicity. From the above scenarios, one can see that *at a given mass, galaxies that are gas-rich (gas-poor) and metal-poor (metal-rich) will have higher (lower) star formation rates.* These trends are qualitatively consistent with observations (Ellison et al. 2008; Lara-López et al. 2010; Mannucci et al. 2010; Peebles & Shankar 2010).

This trend is illustrated for gas fractions and star formation rates by the coloured points in Figure 2, showing that at a given mass, high SFR and high f_{gas} go hand in hand. Figure 1 of DFO11 analogously shows that high SFR accompanies low Z_{gas} at a given M_* . Note that these second-parameter trends do not arise from outflows, being present even in simulations without winds. Instead, it is a direct and unavoidable consequence of equilibrium, and results from galaxies' self-regulating response to fluctuations in inflow rather than any feedback process.

Quantitatively, the scatter around the equilibrium relations depends on how quickly galaxies can return to equilibrium after being perturbed. To return, there must be sufficient infall to re-equilibrate the galaxy. The timescale for this to happen can be quantified by the dilution time (Finlator & Davé 2008):

$$t_{\text{dil}} \equiv \frac{M_{\text{gas}}}{\dot{M}_{\text{in}}} = (1 + \eta)^{-1} \frac{M_{\text{gas}}}{\dot{M}_*} = (1 + \eta)^{-1} t_{\text{dep}}. \quad (14)$$

If the dilution time is small compared to the inflow fluctuation timescale, then the scatter will be small (Finlator & Davé 2008). The inflow fluctuation timescale likely depends on mass and environment, with small galaxies generally suffering (relatively) larger perturbations. Equation 14 shows that the dilution time depends on η and t_{dep} , and hence observations of the scatter versus M_* provides an independent constraint on $\eta(M_*)$ and $t_{\text{dep}}(M_*)$.

Dutton et al. (2010) argues, based on an analytic model of accretion-driven galaxy formation similar to this one, that the scatter in the observed M_* -SFR relation must be driven by fluctuations in inflow, since assuming zero

scatter in the relation between \dot{M}_{in} and M_{halo} results in a relation that is too tight compared to observations. However, hydrodynamic simulations that implicitly include inflow fluctuations also yield a small scatter (e.g. Davé 2008; Finlator, Oppenheimer, & Davé 2011). Therefore it is not solely inflow fluctuations that govern the scatter, it is the more complex relationship between inflow fluctuations and the dilution time. Equation 14 suggests that this, in turn, depends on the outflow rate (η) and gas consumption rate (t_{dep}). The fact that feedback regularizes galaxy properties may have other effects on galaxy properties. For instance, it has long been suggested that the low scatter in the Tully-Fisher relation arises owing to feedback processes, since fluctuations in halo growth alone would naively predict a scatter that is large compared to data (Eisenstein & Loeb 1996).

Satellite galaxies lie permanently off the equilibrium relations, because the inflowing filaments bypass them and flow to the centers of halos. Hence they are expected to end up with lower gas content and higher metallicities than centrals of the same mass; this is as observed (Peebles, Pogge, & Stanek 2009). How far they lie off the equilibrium relations depends on their gas reservoir at the time they are cut off from their supply, which simulations indicate is typically ~ 1 Gyr after falling into a hot gas-dominated halo (Simha et al. 2009). Note that some satellite galaxies fall in along the inflowing filaments, and in those cases they are not bypassed since they are actually part of the inflow. However, these satellites are expected to quickly merge into the central galaxy, and so will not typically end up as part of the long-lived satellite population.

Major mergers are another population lying far out of equilibrium. It is not merely that such systems represent a particularly large inflow perturbation, it is that the induced torques drive gas flows that fuel central star formation (Mihos & Hernquist 1996) making cosmological inflow mostly irrelevant during the merger event. In a global context, major mergers are seen to be responsible for only a small fraction of overall cosmic star formation (e.g. Jogee et al. 2009), although they may be where much of the central black hole mass growth occurs (e.g. Di Matteo et al. 2005). Overall, the equilibrium model is broadly valid for central galaxies that are quiescently forming stars, i.e. main-sequence galaxies (Noeske et al. 2007), that dominate cosmic star formation.

8 BEFORE EQUILIBRIUM: THE GAS ACCUMULATION PHASE

Since the inflow rate has a steeper redshift dependence than the consumption rate (e.g. $\sim (1+z)^{2.25}$ vs. t_H^{-1}), at sufficiently early epochs galaxies will be in a *gas accumulation phase* during which galaxies cannot process gas into stars as fast as they receive it (Bouché et al. 2010; Krumholz & Dekel 2011). Only when consumption can keep up with supply will equilibrium be achieved. During the gas accumulation phase, gas fractions are expected to be higher and metallicities lower than predicted by equilibrium.

We can estimate the redshift z_{eq} where gas accumulation ends and equilibrium is attained. Star formation must be able to occur fast enough to satisfy $\text{SFR} = \dot{M}_{\text{in}}/(1 + \eta)$ (eq. 2). We assume that at early times, $\zeta \approx 1$ and $\alpha_Z \approx 0$,

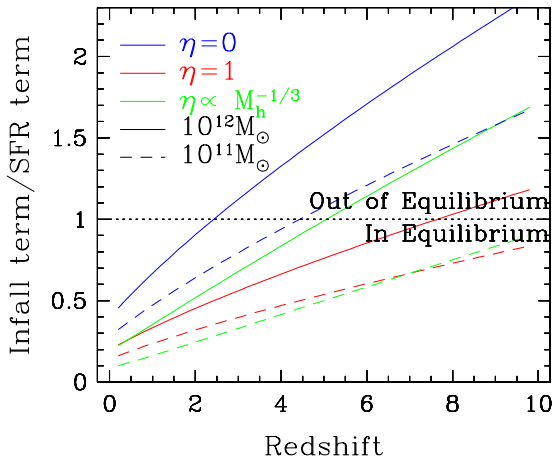


Figure 4. Evolution of the ratio of the infall term (eq. 2) versus the SFR term ($\text{SFR}=0.02M_{\text{gas}}/t_{\text{dyn}}$), for different choices for η and halo mass (solid and dashed lines represent $M_h = 10^{12}$ and $10^{11}M_\odot$, respectively). This calculation assumes $f_{\text{gas}} = 0.5$ for illustration purposes, which is typical at high- z but in detail varies with η and M_h . With no outflows ($\eta = 0$; blue lines), equilibrium for massive galaxies occurs at $z \sim 2$, while less massive galaxies equilibrate earlier. With modest outflows ($\eta = 1$; red lines), equilibrium is already pushed back into the early Universe. The green lines assume momentum-driven wind scalings for η from Oppenheimer & Davé (2008), which pushes equilibrium to $z \sim 5$ for massive galaxies, and much earlier for smaller ones.

so that $\dot{M}_{\text{in}} \approx \dot{M}_{\text{grav}}$ (eq. 3). We further assume that $\text{SFR}=0.02M_{\text{gas}}/t_{\text{dyn}}$, where $t_{\text{dyn}} \approx 10^8(1+z)^{-3/2}$ yr is the disk dynamical time. Taking $M_{\text{gas}} \approx f_{\text{gas}}f_bM_{\text{halo}}$, we obtain an equation for z_{eq} :

$$1 + z_{\text{eq}} \approx \left[5f_{\text{gas}}(1 + \eta) \right]^{4/3} \left(\frac{M_{\text{halo}}}{10^{12}M_\odot} \right)^{-0.2}. \quad (15)$$

We illustrate these trends in Figure 4. For sizeable high- z galaxies with $f_{\text{gas}} \approx 0.4 - 0.5$ (Tacconi et al. 2010) and no outflows ($\eta = 0$), we obtain $z_{\text{eq}} \approx 1.5 - 2.5$, in agreement with Krumholz & Dekel (2011). But the superlinear dependence on f_{gas} and $(1 + \eta)$ means that the results are quite sensitive to these values. For instance, even a modest outflow rate of $\eta = 1$ yields $z_{\text{eq}} \approx 5 - 7$. Effectively, outflows lower the amount of inflow that needs to be processed into stars, allowing for an earlier equilibration epoch. There is a weak halo mass dependence as well such that smaller galaxies equilibrate earlier. Note that this derivation of z_{eq} depends on the star formation law: if the star formation law was different in early galaxies owing e.g. to metallicity effects, then this would also impact when galaxies achieve equilibrium. As such, a precise prediction of z_{eq} is sensitive to poorly known factors. Nevertheless, with realistic outflows, it is likely that $z_{\text{eq}} \gg 2$, and hence galaxies live in equilibrium over the vast majority of cosmic time.

Observationally, Papovich et al. (2010) used the star formation rates, masses, and (estimated) gas contents of high- z Lyman break galaxies to infer that gas accumulation occurs down to $z_{\text{eq}} \sim 4$, after which accretion and star formation track each other as expected in equilibrium. Hence there is some direct empirical support for an early gas accumulation epoch. Constraining z_{eq} more precisely will pro-

vide quantitative constraints on gas processing rates in early galaxies.

9 SUMMARY AND DISCUSSION

We have presented a simple formalism for understanding the evolution of the stellar, gaseous, and metal content of galaxies, inspired by intuition gained from cosmological hydrodynamic simulations. This formalism is encapsulated by the equilibrium relations:

$$\text{SFR} = \frac{\zeta \dot{M}_{\text{grav}}}{(1 + \eta)(1 - \alpha_Z)}, \quad (16)$$

$$f_{\text{gas}} = \frac{1}{1 + (t_{\text{dep}}\text{SFR})^{-1}}, \quad (17)$$

$$Z_{\text{ISM}} = \frac{y}{1 + \eta} \frac{1}{1 - \alpha_Z}. \quad (18)$$

These relations are established by a balance between inflows and outflows, and evolve on cosmological timescales over which inflow and outflow rates slowly vary. They are primarily governed by three baryon cycling parameters that describe ejective feedback (η), preventive feedback (ζ), and the re-accretion of ejected material (α_Z); each of these parameters is in principle directly observable, but at present has poorly known dependences on mass and redshift (and perhaps other properties). Additionally, they depend on \dot{M}_{grav} , the gravitational infall rate of baryons into the halo set by Λ CDM, t_{dep} , the ISM gas depletion time, and y , the metal yield. These relations capture, to first order, the behavior of galaxies in modern hydrodynamic simulations that incorporate these processes dynamically within a hierarchical structure formation scenario.

The equilibrium model is broadly valid for quiescently star-forming central galaxies, at epochs where star formation is able to keep up with inflow (i.e. past the gas accumulation epoch; Figure 4), and when averaged over timescales longer than stochastic fluctuations in the inflow rate. On shorter timescales, galaxies oscillate around the equilibrium relations such that more (less) rapidly star-forming galaxies at a given mass having higher (lower) gas fractions and lower (higher) metallicities. The scatter about the relations is governed by a competition between the dilution time $t_{\text{dil}} = (1 + \eta)^{-1}t_{\text{dep}}$ and the inflow stochasticity timescale. This model is *not* valid for satellite galaxies disconnected from feeding filaments, or for galaxies undergoing a major merger where gas feeding is temporarily driven by internal dynamical processes. Nonetheless, observations indicate that quiescently star-forming galaxies along the so-called galaxy main sequence dominate cosmic star formation at all epochs where measured (e.g. Noeske et al. 2007; Rodighiero et al. 2011), and hence this model describes how the bulk (but not all) of the stars in the Universe formed.

Most current galaxy formation models, both hydrodynamic and semi-analytic, already include inflow and outflow processes within growing large-scale structure. Hence there is no new physics in the equilibrium model. What is notable is not what this scenario contains, but rather what it *doesn't* contain. In particular, there is no explicit mention of mergers, disks, environment, cooling radii, or virial radii—all central elements in the canonical scenario for galaxy formation. Such elements are automatically accounted for in

hydrodynamic simulations, which form disks, merge them, and implicitly include environmental effects within growing large-scale structure. Yet the equilibrium relations well describe such simulations without reference to these elements, suggesting that they are not of primary importance for the evolution of galaxies' SFR, f_{gas} , and Z .

In a broader context, the usefulness of the equilibrium scenario is that it lays bare the overwhelming complexity of modern galaxy formation models, and isolates those aspects that are critical for governing global galaxy evolution, thereby providing a simpler intuitive view for how galaxies grow. Although the canonical “halo-merger” view of disks cooling within halos and merging to drive galaxy evolution is not incorrect (i.e. these processes do happen), such a view obfuscates the primary driver of global galaxy evolution, namely the balance between inflows, outflows, and star formation. Indeed, the very notion of a galaxy halo, which is central to the classical view of galaxy formation, is only a second-order effect in the equilibrium scenario: The equilibrium relations are driven by the total inflow rate, and the “lumpiness” of that inflow owing to individual halos merely manifests as scatter around these relations.

We have argued that the equilibrium model provides a reasonable description of sophisticated simulations, but this in no way guarantees that it accurately describes the real Universe. It is encouraging that certain unavoidable predictions such as continual gas replenishment and the second-parameter dependence of the mass-metallicity relation seem to be in broad agreement with observations. But much work remains to be done in order to fully test this scenario. In particular, the equilibrium model centrally invokes a continual cycle of baryons flowing in and out of galaxies as a key moderator of galaxy evolution. But direct observational evidence for such processes is currently scant (see e.g. Rubin et al. 2011). Critically testing and constraining these baryon cycling processes, particularly within circum-galactic gas where such processes are likely to be most prominent, will be a key contribution from upcoming multi-wavelength observational facilities.

The equilibrium model provides a re-parameterized framework for understanding certain key governing aspects of galaxy evolution, but is far from a full solution to the problem. To fully solve galaxy evolution, we must at minimum understand the physics that governs η , ζ , and α_Z , which will require concerted efforts on both observational and theoretical fronts. Furthermore, halo accretion rates, metal yields, and the star formation law remain uncertain, particularly in regimes such as small low-metallicity galaxies. Perhaps most importantly, this scenario in its current form explicitly does not address many interesting aspects of galaxy evolution such as the establishment of the Hubble sequence and the growth of central black holes. It also does not include processes that may be central to the evolution of certain classes of galaxies; for instance, it does not account for stellar (“dry”) mergers which are important for the late-time growth of large passive systems. Hence much work remains to be done in order to comprehensively understand how galaxies evolve from primordial fluctuations into their present state. It is hoped that the equilibrium model provides, in its simplicity, a useful guiding framework for understanding the increasingly complex problem of galaxy evolution.

ACKNOWLEDGEMENTS

The authors thank N. Bouché, A. Dekel, R. Genzel, N. Katz, D. Kereš, A. Loeb, N. Murray, C. Papovich, E. Quataert, J. Schaye, L. Tacconi, and D. Weinberg for helpful discussions. This work was supported by the National Science Foundation under grant numbers AST-0847667 and AST-0907998. Computing resources were obtained through grant number DMS-0619881 from the National Science Foundation.

REFERENCES

- Benson, A. J. 2010, *PhR*, 495, 33
 Bolatto, A. D. et al. 2011, *ApJ*, in press, arXiv:1107.1717
 Bouche, N. et al. 2010, *ApJ*, 718, 1001
 Bresolin, F., Ryan-Weber, E., Kennicutt, R. C., Goddard, Q. 2009, *ApJ*, 695, 580
 Brooks, A. M. et al. 2007, *ApJL*, 655, L17
 Cattaneo, A., Mamon, G. A., Warnick, K., Knebe, A. 2011, *A&A*, 533, 5
 Chabrier G., 2003, *PASP*, 115, 763
 Croton, D. J. et al. 2006, *MNRAS*, 365, 11
 Daddi, E. et al. 2007, *ApJ*, 670, 156
 Davé, R., Finlator, K., Oppenheimer, B. D. 2006, *MNRAS*, 370, 273
 Davé, R. 2008, *MNRAS*, 385, 147
 Davé, R., Oppenheimer, B. D., Finlator, K. M. 2011, *MNRAS*, in press
 Davé, R., Finlator, K. M., Oppenheimer, B. D. 2011, *MNRAS*, in press (DFO11)
 Dekel, A. & Silk, J. 1986, *ApJ*, 303, 39
 Dekel, A. & Birnboim, Y. 2006, *MNRAS*, 368, 2
 Dekel, A. et al. 2009, *Nature*, 457, 451
 Di Matteo, T., Springel, V., Hernquist, L. 2005, *Nature*, 433, 604
 Dutton, A. A., van den Bosch, F. C., Dekel, A. 2010, *MNRAS*, 405, 1690
 Eisenstein, D. J., Loeb, A. 1996, *ApJ*, 459, 432
 Ellison, S. L., Patton, D. R., Simard, L., McConnachie, A. W. 2008, *ApJL*, 672, L107
 Erb, D. K., Shapley, A. E., Pettini, M., Steidel, C. C., Reddy, N. A., Adelberger, K. L. 2006, *ApJ*, 644, 813
 Fakhouri, O., Ma, C.-P., Boylan-Kolchin, M. 2010, *MNRAS*, 406, 2267
 Faucher-Giguere, C. A., Kereš, D., Ma, C.-P. 2011, *MNRAS*, submitted, arXiv:1103.0001
 Finlator, K. & Davé, R. 2008, *MNRAS*, 385, 2181
 Finlator, K., Oppenheimer, B. D., Davé, R. 2011, *MNRAS*, 410, 1703
 Finlator, K., Davé, R., Özel, F. 2011, *ApJ*, submitted, arXiv:1106.4321
 Gabor, J. M., Davé, R., Finlator, K., Oppenheimer, B. D. 2011, *MNRAS*, in press
 Geach, J. E., Smail, I., Moran, S. M., MacArthur, L. A., Lagos, C. d. P., Edge, A. C. 2011, *ApJL*, 730, L19
 Genel, S., Bouché, N., Naab, T., Sternberg, A., Genzel, R. 2010, *ApJ*, 719, 229
 Genzel, R. et al. 2010, *MNRAS*, 407, 2091
 Genzel, R. et al. 2011, *ApJ*, 733, 101
 Gnedin, N. Y. 2000, *ApJ*, 542, 535
 González, V., Labbé, I., Bouwens, R. J., Illingworth, G.,

- Franx, M., Kriek, M., Brammer, G. B. 2010, *ApJ*, 713, 115
- Graham, A. W., Onken, C. A., Athanassoula, E., Combes, F. 2011, *MNRAS*, 412, 2211
- Grogin, N. A. et al. 2011, *ApJS*, submitted, arXiv:1105.3753
- Gultekin, K. et al. 2009, *ApJ*, 698, 198
- Hopkins, P. F., Hernquist, L., Cox, T. J., Kereš, D. 2008, *ApJS*, 175, 390
- Jogee, S. et al. 2009, *ApJ*, 697, 1971
- Katz, N., Weinberg, D. H., Hernquist, L. 1996, *ApJS*, 105, 19
- Kennicutt, R. C. 1998, *ApJ*, 498, 541
- Kereš, D., Katz, N., Weinberg, D. H., & Davé, R. 2005, *MNRAS*, 363, 2
- Koekemoer, A. M. et al. 2011, *ApJS*, submitted, arXiv:1105.3754
- Krumholz, M. R., Tan, J. C. 2007, *ApJ*, 654, 304
- Krumholz, M. R., Dekel, A. 2011, *ApJ*, submitted, arXiv:1106.0301
- Lara-López, M. A. et al. 2010, *A&A*, 521, L53
- Lee, H., Skillman, E. D., Cannon, J. M., Jackson, D. C., Gehr, R. D., Polonski, E. F., Woodward, C. E. 2006, *ApJ*, 647, 970
- Mannucci, F., Cresci, G., Maiolino, R., Marconi, A., Gnerucci, A. 2010, *MNRAS*, 408, 2115
- McBride, J., Fakhouri, O., Ma, C.-P. 2009, *MNRAS*, 398, 1858
- Mihos, J. C. & Hernquist, L. 1996, *ApJ*, 464, 641
- Mo, H. J., Mao, S., White, S. D. M. 1998, *MNRAS*, 295, 319
- Moran, S. M. et al. 2011, *ApJ*, submitted
- Murray, N., Quatert, E., Thompson, T. A. 2005, *ApJ*, 618, 569
- Neistein, E., van den Bosch, F. C., Dekel, A. 2006, *MNRAS*, 372, 993
- Neistein, E., Dekel, A. 2008, *MNRAS*, 388, 1792
- Neistein, E., Khochfar, S., Dalla Vecchia, C., Schaye, J. 2011, *MNRAS*, submitted, arXiv:1109.4635
- Noeske, K. G. et al. 2007, *ApJL*, 660, L43
- Ocvirk, P., Pichon, C., Teyssier, R. 2008, *MNRAS*, 390, 1326
- Okamoto, T., Gao, L., Theuns, T. 2008, *MNRAS*, 390, 920
- Oppenheimer, B. D., Davé, R., Kereš, D., Katz, N., Kollmeier, J. A., Weinberg, D. H. 2010, *MNRAS*, 406, 2325
- Oppenheimer, B. D. & Davé, R. 2008, *MNRAS*, 387, 577
- Oppenheimer, B. D., Davé, R., Katz, N., Kollmeier, J. A., Weinberg, D. H. 2011, *MNRAS*, submitted, arXiv:1106.1444
- Papovich, C., Finkelstein, S. L., Ferguson, H. C., Lotz, J. M., Giavalisco, M. 2010 *MNRAS*, 412, 1123
- Pawlik, A. H., Schaye, J., *MNRAS*, 396, L46
- Peeples, M. S., Pogge, R. W., Stanek, K. Z. 2009, *ApJ*, 695, 259
- Peeples, M. S., Shankar, F. 2010, *MNRAS*, accepted, arXiv:1007.3743
- Rasera, Y. & Teyssier, R. 2006, *A&A*, 445, 1
- Rees, M. J., & Ostriker, J. P. 1977, *MNRAS*, 179, 541
- Rodighiero, G. et al. 2011, *ApJ*, 739, L40
- Rubin, K. H. R., Prochaska, J. X., Koo, D. C., Phillips, A. C. 2011, *ApJL*, submitted, arXiv:1110.0837
- Salim, S. 2007, *ApJS*, 173, 267
- Schaye, J. et al. 2010, *MNRAS*, 402, 1536
- Silk, J. 1997, *ApJ*, 481, 703
- Simha, V., Weinberg, D. H., Davé, R., Gnedin, O. Y., Katz, N., Kereš, D. 2009, *MNRAS*, 299, 650
- Somerville, R. S., Hopkins, P. F., Cox, T. J., Robertson, B. E., Hernquist, L. 2008, *MNRAS*, 391, 481
- Springel, V. & Hernquist, L. 2003, *MNRAS*, 339, 312
- Steidel, C. C. et al. 2010, *ApJ*, 717, 298
- Tacconi, L. J. et al. 2010, *Nature*, 463, 781
- Thoul, A. A., Weinberg, D. H. 1996, *ApJ*, 465, 608
- Tremonti, C. A. et al. 2004, *ApJ*, 613, 898
- Tully, R. B., Fisher, J. R. 1977, *A&A*, 54, 661
- van de Voort, F., Schaye, J., Booth, C. M., Haas, M. R., Dalla Vecchia, C. 2011, *MNRAS*, 414, 2458
- White, S. D. M., & Rees, M. J. 1978, *MNRAS*, 183, 341
- White, S. D. M. & Frenk, C. S. 1991, *ApJ*, 379, 52